

## SUPPORTING INFORMATION

### Metallic Nanoporous Aluminum-Magnesium Alloy for UV Enhanced Spectroscopy

*Paolo Ponzellini<sup>1</sup>, Giorgia Giovannini<sup>1</sup>, Sandro Cattarin<sup>2</sup>, Remo Proietti Zaccaria<sup>1,3</sup>, Sergio Marras<sup>1</sup>, Mirko Prato<sup>1</sup>, Andrea Schirato<sup>4</sup>, Francesco D'Amico<sup>5</sup>, Eugenio Calandrini<sup>1</sup>, Francesco De Angelis<sup>1</sup>, Wei Yang<sup>6</sup>, Hai-Jun Jin<sup>6</sup>, Alessandro Alabastri<sup>4</sup>, and Denis Garoli<sup>1\*</sup>*

<sup>1</sup> Istituto Italiano di Tecnologia, via Morego 30, I-16163, Genova, Italy.

<sup>2</sup> ICMATE - CNR, Corso Stati Uniti 4, 35127 Padova, Italy.

<sup>3</sup> Cixi Institute of Biomedical Engineering, Ningbo Institute of Industrial Technology, Chinese Academy of Sciences, 1219 Zhongguan West Road, Ningbo 315201 P.R. China.

<sup>4</sup> Electrical and Computer Engineering, Rice University, 6100 Main Street MS-378, Houston, TX 77005

<sup>5</sup> Elettra Sincrotrone Trieste in Area Science Park, S.S. 14 Km 163,5 34012 Basovizza (TS) Italy

<sup>6</sup> Shenyang National Laboratory for Materials Science, Institute of Metal Research, Chinese Academy of Sciences, 72 Wenhua Road, Shenyang 110016 P.R. China

\* Corresponding author: Dr. Denis Garoli, [denis.garoli@iit.it](mailto:denis.garoli@iit.it);

#### Supporting Note #1 – Dealloying process

With the aim of obtaining a less oxidized porous material, we have performed the dealloying process with several different acids and on different pristine alloy samples. Unfortunately no acid guaranteed a lower oxidation, in the etched sample, with respect to acetic acid. Here are reviewed our attempts, with the SEM images and the EDS compositional analyses relative to every acid.

##### - Acetic acid (CH<sub>3</sub>COOH)

Following the etching procedure reported in the main text we verified what happen increasing the initial amount of Al in the alloy (compare Table 1).

<i>Sample (Al-Mg sputtering power W)</i>	<i>Pristine composition x (Al<sub>x</sub>Mg<sub>1-x</sub>)*</i>	<i>(EDS) Etched composition (O, Al, Mg)</i>
E (100-55)	0.35	21%,35%,44%

Sample E has been prepared by co-sputtering of Al and Mg at powers of 100 W and 55 W, respectively. The etching process has been performed for 5 minutes. The porous morphology of the etched sample is depicted in Fig. S1(E1)(E2). As can be observed, 5 minutes were not enough for the acid solution to penetrate through the whole of the sample thickness. Only a superficial layer (at the bottom area of Fig. S1(E2)) results etched, and then porous. This suggests that an excess of Al

in the starting alloy makes the etching slower/more difficult and causes a higher level of oxidation, as demonstrated from the EDS measurement.

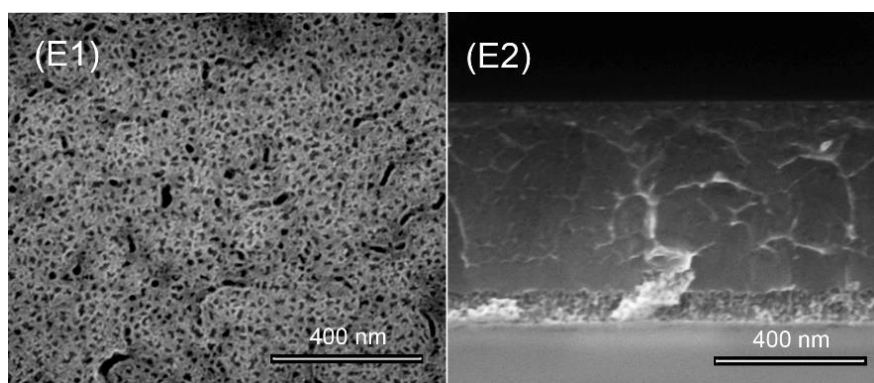


**Figure S1.** SEM micrographs of the prepared sample E. Top and cross-section view.

- **Ammonium acetate ( $\text{C}_2\text{H}_7\text{NO}_2$ )**

We performed our dealloying procedure with a solution of 1M ammonium acetate. The solution resulted less aggressive, and then slower in removing Mg, than the acetic acid one. The results, in terms of composition of the porous material, anyway were similar.

<i>Pristine composition <math>x</math> (<math>\text{Al}_x\text{Mg}_{1-x}</math>)</i>	<i>Final composition (O, Al, Mg)</i>	<i>Etching time</i>
0.41	34%, 37%, 29%	4 h

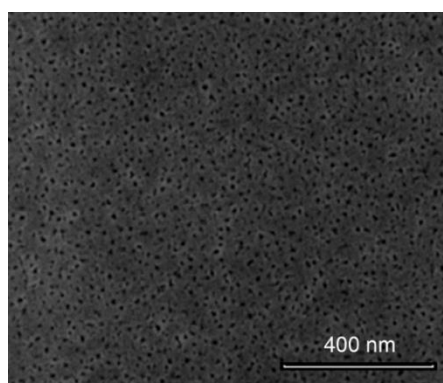


**Figure S2.** Ammonium acetate etched sample. SEM micrograph

- **Phosphoric acid ( $\text{H}_3\text{PO}_4$ )**

We performed our dealloying procedure with a 5.2 vol% concentrated  $\text{H}_3\text{PO}_4$ . Unfortunately the acid solution rapidly dissolved the  $x=0.74$  pristine  $\text{Al}_x\text{Mg}_{1-x}$  alloy; or at least detached it from the silicon substrate. We found a non-uniform, very thin layer of Al, on the substrate (Fig.S3)

<i>Pristine composition <math>x</math> (<math>\text{Al}_x\text{Mg}_{1-x}</math>)</i>	<i>Final composition (O, Al, Mg)</i>	<i>Etching time</i>
0.26	60%, 39%, 1%	Few seconds

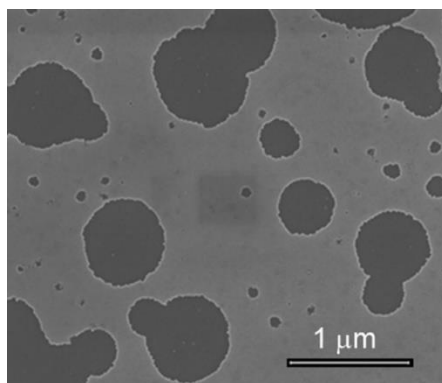


**Figure S3.** Phosphoric acid etched sample. Only some of the linker Al layer is left on the silicon substrate. SEM micrograph.

- **Sulphuric acid ( $\text{H}_2\text{SO}_4$ )**

The Al-Mg alloy, annealed at  $450^\circ\text{C}$  for one hour after the sputter deposition, was treated in diluted sulphuric acid solution ( $\text{H}_2\text{SO}_4$  vol. 0.38%). The composition of the etched sample resulted similar to the acetic acid ones. Fig. S4 illustrates the obtained morphology.

<i>Pristine composition <math>x</math> (<math>\text{Al}_x\text{Mg}_{1-x}</math>)</i>	<i>Final composition (O, Al, Mg)</i>	<i>Etching time</i>
0.34, annealed sample ( $450^\circ\text{C}$ )	44%,38%, 18%	40 sec

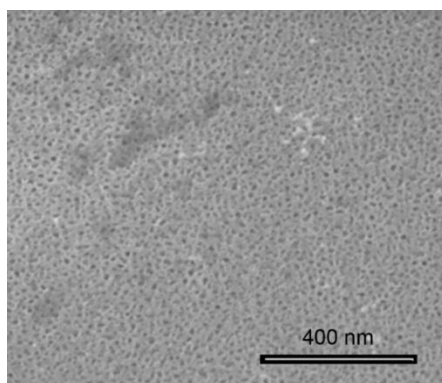


**Figure S4.** 0.34% Al rich, annealed sample ( $450^\circ\text{C}$ ), etched for 40 seconds in sulphuric acid. SEM micrograph.

- **Citric acid ( $\text{C}_6\text{H}_8\text{O}_7$ )**

We performed the dealloying procedure with a 1M solution of  $\text{C}_6\text{H}_8\text{O}_7$ . The result was not satisfying. After pulling out the sample from the acid solution, we weren't able to get rid of the acid solution trapped inside the porous material, not even by rinsing the sample in pentane.

<i>Pristine composition <math>x</math> (<math>\text{Al}_x\text{Mg}_{1-x}</math>)</i>	<i>Final composition (C, O, Al, Mg)</i>	<i>Etching time</i>
0.26	17%,45%,35%, 3%	4 h 20 min.

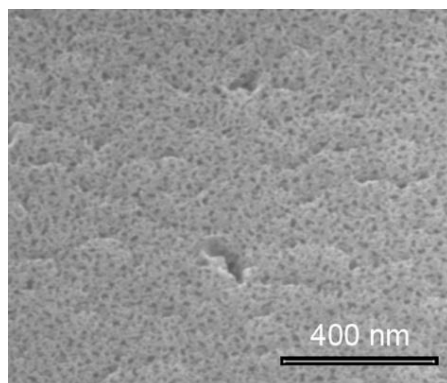


**Figure S5.** Sample etched in citric acid. SEM micrograph.

## Supporting Note #2 - EDS spectrum.

We acquired the EDS spectra from at least five positions for each sample. For each element, the composition percentages measured in different areas differed one from the other by less than 1%, which together to the homogeneity of the sample, convinced us of the reproducibility of our measurements.

### Sample A<sub>0</sub>

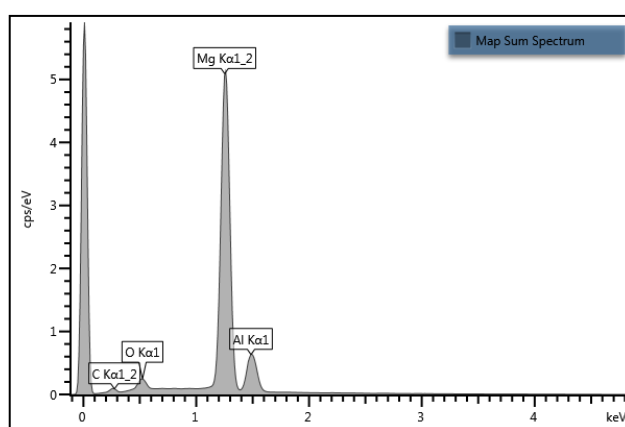


**Figure S6.** Sample A<sub>0</sub> - EDS spectrum.

### Sample B<sub>1</sub> and B<sub>2</sub>

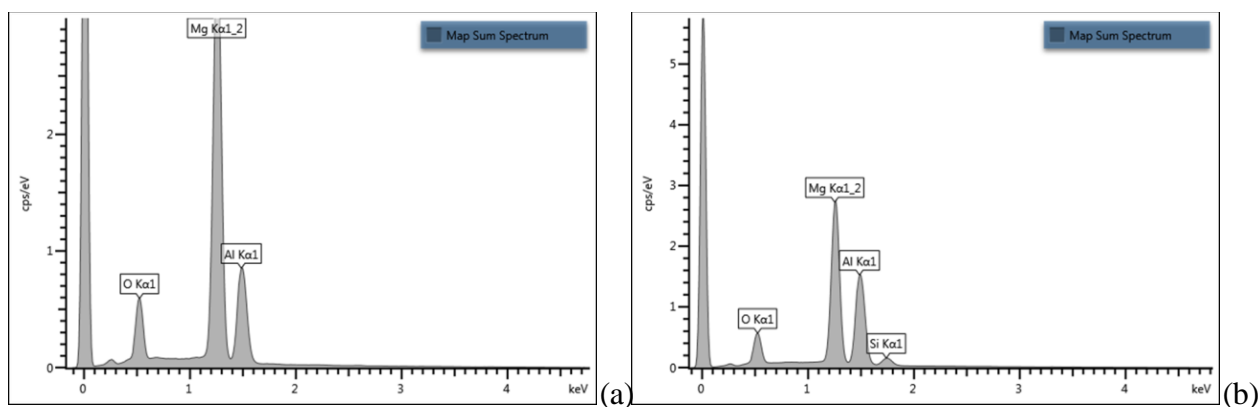


**Figure S7.** EDS spectra. (a) Sample B<sub>1</sub>; (b) Sample B<sub>2</sub>.

## Sample C<sub>1</sub>

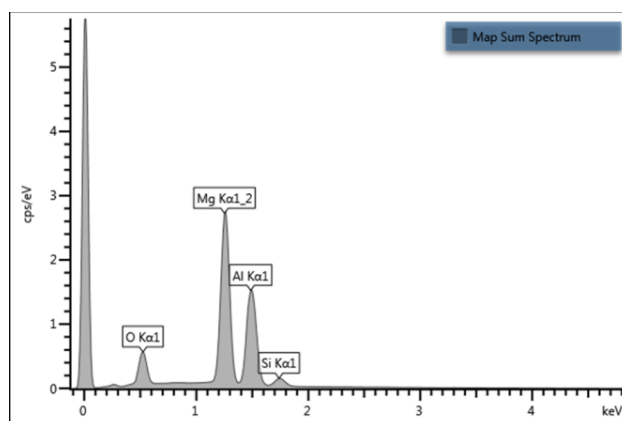


**Figure S8.** Sample C<sub>1</sub> - EDS spectrum

## Supporting Note #3 – XPS analyses

The strong reactivity of both Al and Mg, both in air and in the etching solutions, determines the oxidation of the surface of all the obtained samples. Even though both EDS and XRD investigations could demonstrate that the bulk composition is prevalently metallic, additional investigations have been performed in order to evaluate the surface film oxygen content. This analysis has been performed through XPS technique. Table S1 reports a summary of the obtained data (details of the measured spectrum are reported below).

**Table S1.** Samples, XPS analyses.

Sample	Al <sub>2</sub> O <sub>3</sub> (at%)	Al suboxides (at%)	Metallic Al	MgO	Metallic Mg
A <sub>0</sub>	5%	0	6%	71%	18%
B <sub>1</sub>	15%	6%	9%	10%	60%
B <sub>2</sub>	41%	5%	10%	5%	39%
C <sub>1</sub>	59%	6%	13%	20%	2%

\*For sample 135-100 pristine, the Al peak overlaps with the secondary peaks that are related to the high Mg content. The quantification may not be accurate, but some metallic Al is certainly present.

The results confirm what previously observed. A longer dealloying time implies higher surface oxidation, mainly in form of Al oxides. The pre-alloying annealing reduces the amount of metallic Mg in the final sample while slightly increasing the amount of Mg oxide. In all the samples, the metallic Al within the first few nm of the film is below 14% while higher amounts of metallic Mg are observed in samples B<sub>1</sub> and B<sub>2</sub>. The main oxide, in all the etched samples, is Al<sub>2</sub>O<sub>3</sub> while MgO seems to be dominant in the case of sample A<sub>0</sub>.

Here we report on recorded XPS spectrum.

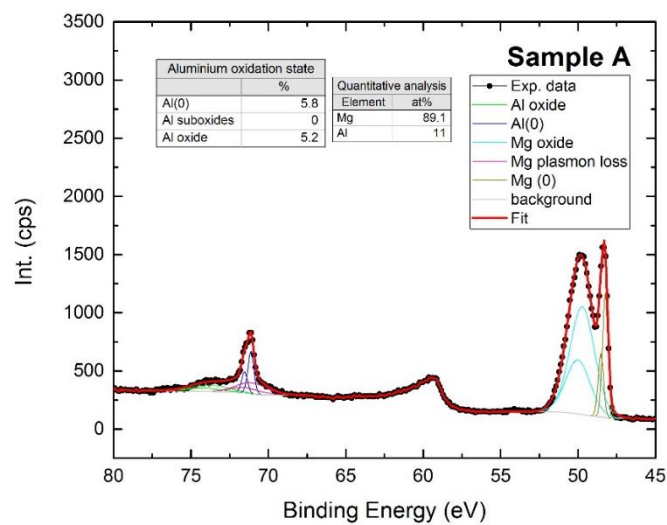


Figure S9. XPS analysis for Sample A<sub>0</sub>.

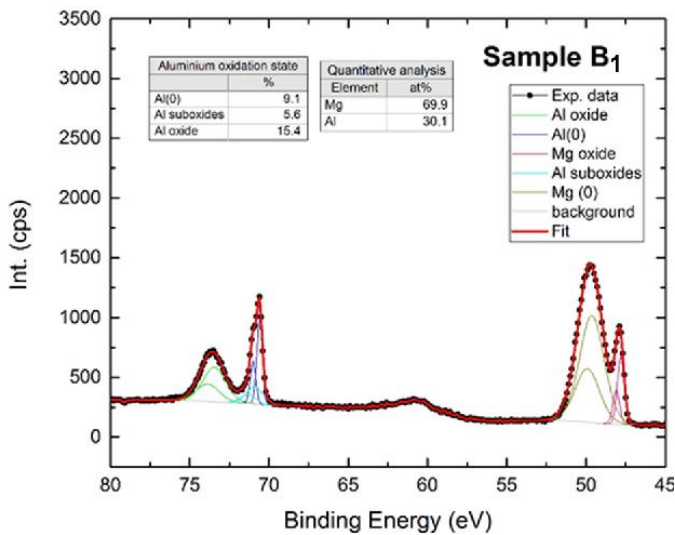
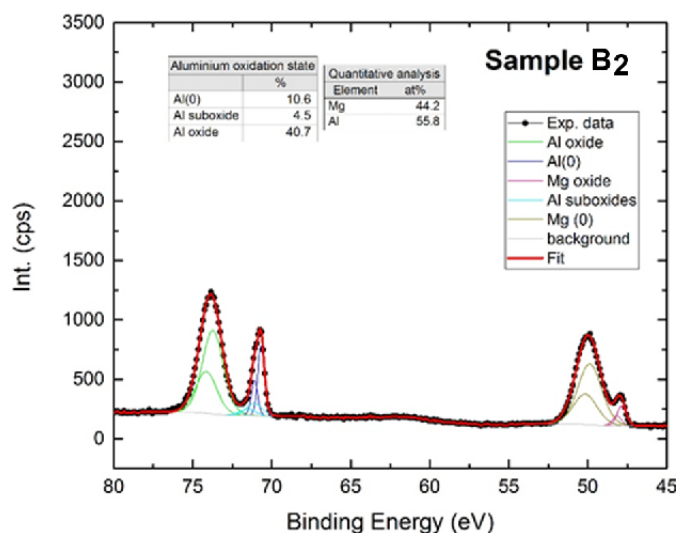
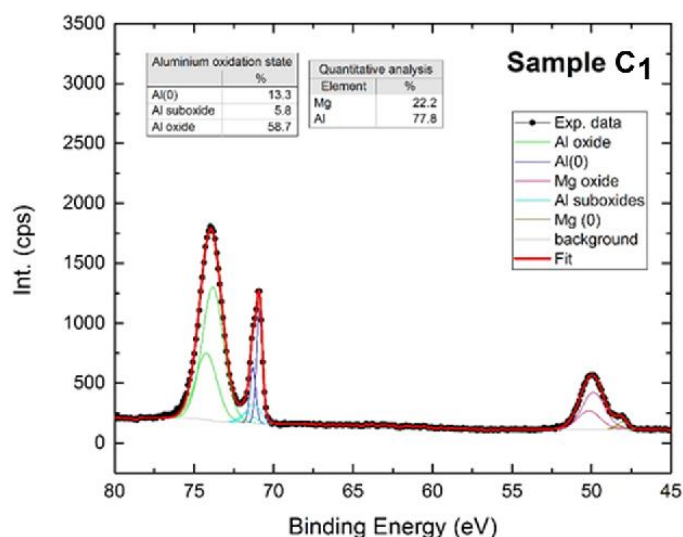


Figure S10. XPS analysis for Sample B<sub>1</sub>.



**Figure S11.** XPS analysis for Sample B<sub>2</sub>.



**Figure S12.** XPS analysis for Sample C<sub>1</sub>.

#### Supporting Note #4 – Dielectric constants

Following a procedure recently used for NPG (see Ref. 39 main text), a Drude – Lorentz model based fit has been performed on the reflectance spectrum in order to obtain an estimation of the dielectric constants of samples (Fig. S13) and their metallic properties for plasmonic applications. Since it has not been possible to achieve a reasonable fit from R data of sample B<sub>2</sub> and C<sub>1</sub> we report only results for sample A<sub>0</sub> and B<sub>1</sub>. This procedure is here reported as a preliminary evaluation of the dielectric constants of the NPAM samples. The high roughness make reflectance (and also ellipsometric) measurements challenging, consequently, the dielectric constants have been extracted from total reflectance (specular+ diffuse) measurements performed by means of a spectrophotometer equipped with an integrating sphere. Noteworthy, in NPAM samples it's not possible to observe the interband peak of Al at 800 nm. This can be explained because our NPAM

are an alloy of AlMg where Mg is dominant (the composition is close to  $\text{Al}_x\text{Mg}_{1-x}$  with  $x=0.3$ ). Mg is known to be a perfect Hermitian metal (see Caligiuri et al. Nano Letters (2019) DOI:10.1021/acs.nanolett.9b00564) and we expect that its high reflectance in the VIS/NIR can make the interband transition of Al extremely weak to be detected.

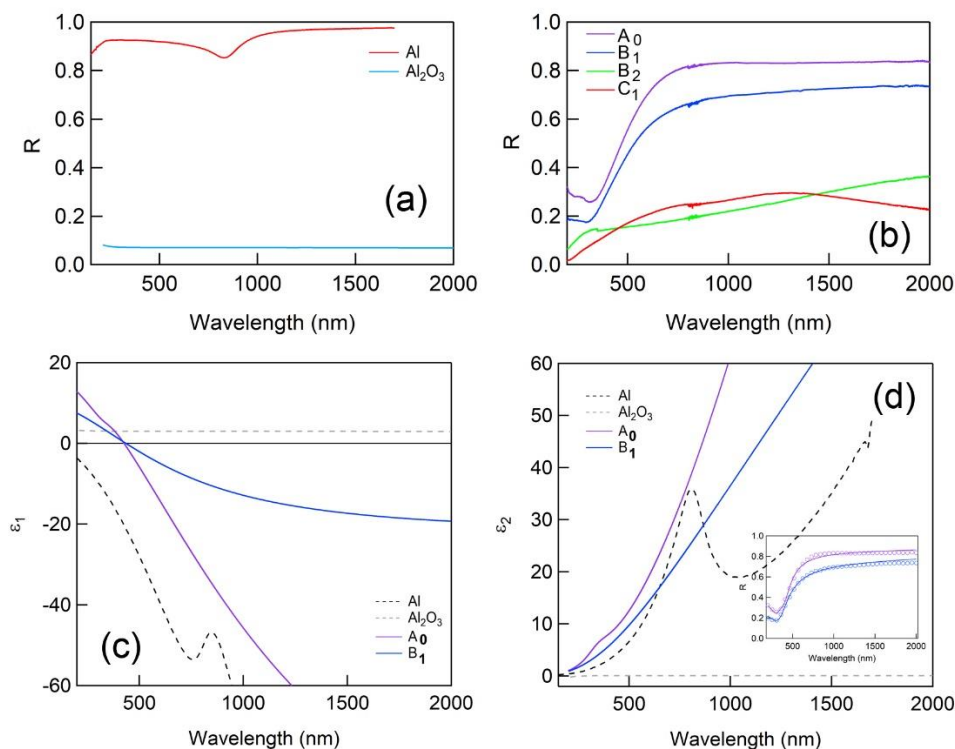


**Figure S13.** Integrated reflectance spectrum and Dielectric Constants as obtained from a Drude-Lorentz best-fit. (a) Data from bulk Al and  $\text{Al}_2\text{O}_3$  samples; (b) Integrated Reflectance from NPAM samples; (c-d) Dielectric constants obtained from best-fit for sample  $A_0$  and  $B_1$  (inset: comparison between fit and experimental data).

## Supporting Note #5 – Substrate functionalization

### - Substrates functionalization with activated coumarin derivative.

The substrates were firstly treated with APTES ((3-Aminopropyl)triethoxysilane) in order to expose amino groups on the surface which are subsequently used as anchors to covalently attach the carboxylated-coumarin previously activated using EDC-NHS as coupling agents.



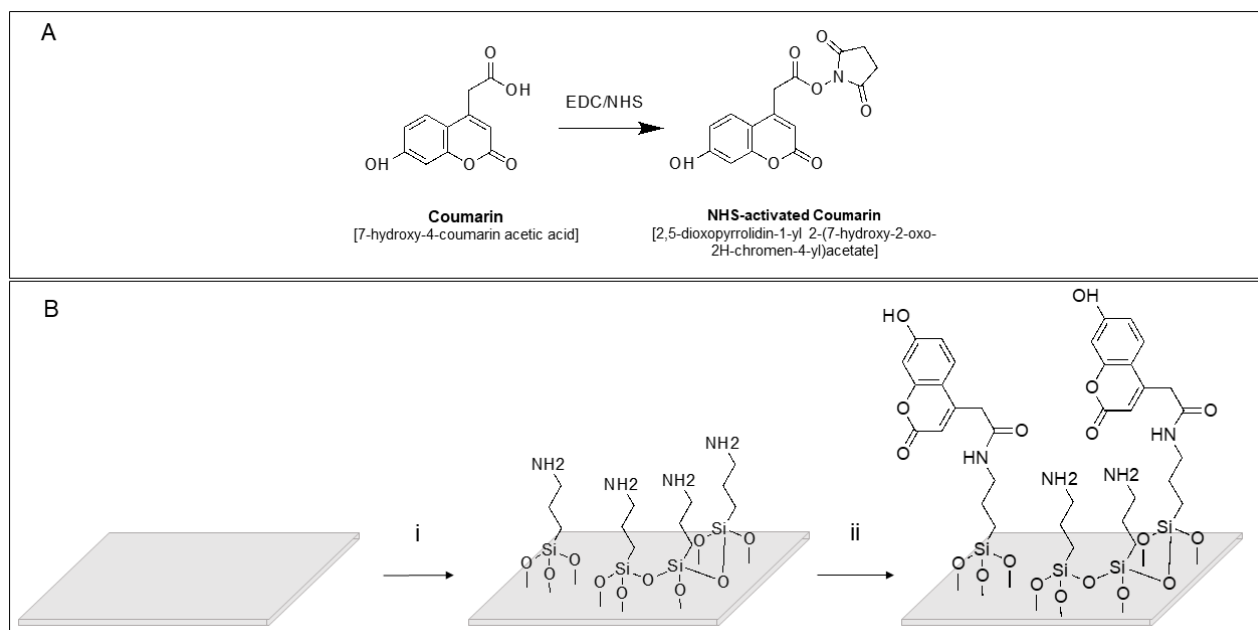


**Figure S14:** A) Dye activation by EDC/NHS coupling reagents: Coumarin, EDC (in DMSO) stirred under controlled conditions for 15 minutes. NHS is added and the reaction is stirred for other 45 minutes. B) Surface functionalisation: i) treated surface, 4% APTES (in acetone), overnight under controlled conditions. ii) APTES-functionalised surface, NHS-activated coumarin (1 mM, acetone) overnight under controlled conditions. Controlled conditions: argon atmosphere,  $H_2O < 0.1$  ppm;  $O_2 < 0.1$  ppm, RT.

In Table S2 we report about the amount of coumarin dyes attached on our samples and on the fluorescence properties of such functionalized samples.

**Table S2:** The measured Coumarin concentration ( $\mu\text{M}$ ) and fluorescence signal are reported for each sample. The Fluorescence Enhancement (FE), then is calculated for each substrate as the ratio between the fluorescence intensity and the concentration of the fluorophore.

	Coumarin conc. (CC)		Fluorescence intensity (FI)		FE	
	( $\mu\text{M}$ )	Relative to sample B <sub>1</sub> (%)	(A.U.)	Relative to sample A <sub>0</sub> (%)	FI/CC	Relative to sample Al
A <sub>0</sub>	90.69	61	19788	100	218.20	9.51
B <sub>1</sub>	147.50	100	4750	24	32.20	1.40
B <sub>2</sub>	38.24	26	3744	19	97.91	4.27
C <sub>1</sub>	72.70	49	5373	27	73.91	3.22
Al	105.03	71	2410	12	22.94	1.00

#### - Substrates functionalization with CsPbBr<sub>3</sub> colloidal Nanocrystal

Under controlled conditions (argon atmosphere,  $\text{H}_2\text{O} < 0.1$  ppm;  $\text{O}_2 < 0.1$  ppm, RT.), 2.5  $\mu\text{L}$  of CsPbBr<sub>3</sub> colloidal Nanocrystals (NCs) solution ( $6.5 \times 10^{14}$  NCs/mL in toluene) were dropped on substrate A<sub>0</sub>, and rough Al (Al) ensuring that all the suspension remained on the substrate to guarantee that the same amount of NCs was deposited on all substrates. Synthesis and fluorescence properties of NCs used in this experiment are described elsewhere (Ref. 46 main text). After solvent evaporation, the fluorescence spectrum of the substrates was recorded by exciting at a wavelength of 280 nm and observing a fluorescence peak at 510 nm (Figure S15). The signal measured for Al was used as the reference. The FE property of A<sub>0</sub> is confirmed: the signal measured at 510 nm (17734 A.U.) is 6-fold higher in comparison to the fluorescence measured for Al (3003 A.U.) Such a comparison highlights the intriguing properties of the NPAM samples. Noteworthy, these NCs have a quantum efficiency close to 1, so the observed enhancement is reasonably due to an enhanced absorption of the exciting light of the substrate.

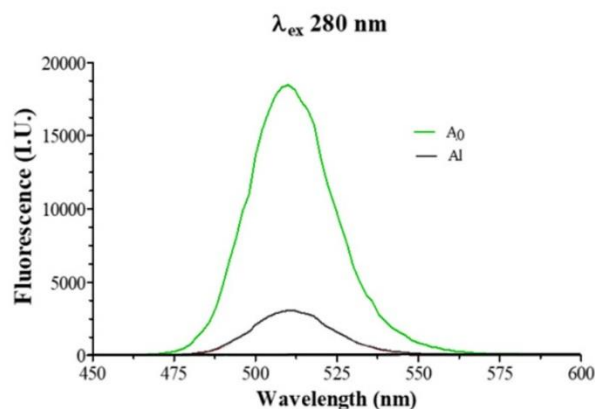


**Figure S15:** Fluorescence measurement of NCs deposited on substrates after toluene evaporation. Fluorescence spectrum measured for each substrate tested ( $\lambda_{ex}$  280 nm).

#### Supporting Note #6 – Fluorescence measurement on rough Al with and without SiO<sub>2</sub> layer.

Here we report a comparison between the fluorescence measurement performed on the reference “Al” sample coated with SiO<sub>2</sub> and without this protective layer. In the latter case, the Al film presents a self-passivation layer of Al<sub>2</sub>O<sub>3</sub>. The measurements have been performed after the functionalization with Coumarin derivate following the procedure reported in SI#5. The obtained FI seems to demonstrate that no significant difference exist between the two substrates.

**Table S3:** The measured Coumarin concentration ( $\mu\text{M}$ ) and fluorescence signal are reported for 10 nm thick rough Aluminum with and without SiO<sub>2</sub> layer.

	Coumarin conc. (CC)	Fluorescence intensity (FI)
	( $\mu\text{M}$ )	(A.U.)
Al (Al <sub>2</sub> O <sub>3</sub> self-passivation)	98.55	2475
Al (SiO <sub>2</sub> )	115.90	2750

## Supporting Note #7 – Numerical Analysis

The numerical analysis presented and discussed in Fig. 5 of the main text have been performed more extensively, in order to investigate the spectral features of the optical response of the system as well as the impact of the main parameters on the results.

In particular, simulations have been conducted on samples  $A_0$  and  $C_1$  at different wavelengths (260 nm and 360 nm) in order to compare the numerically-computed field enhancement distribution with the results from fluorescence measurements. Figure S16 illustrates the calculation of the field distribution for sample  $A_0$ . Please, note that the illustrated sample morphology is representative of the roughness of the sample, but it's not a nanoporosity. The sample, in fact, has been cleaved mechanically.

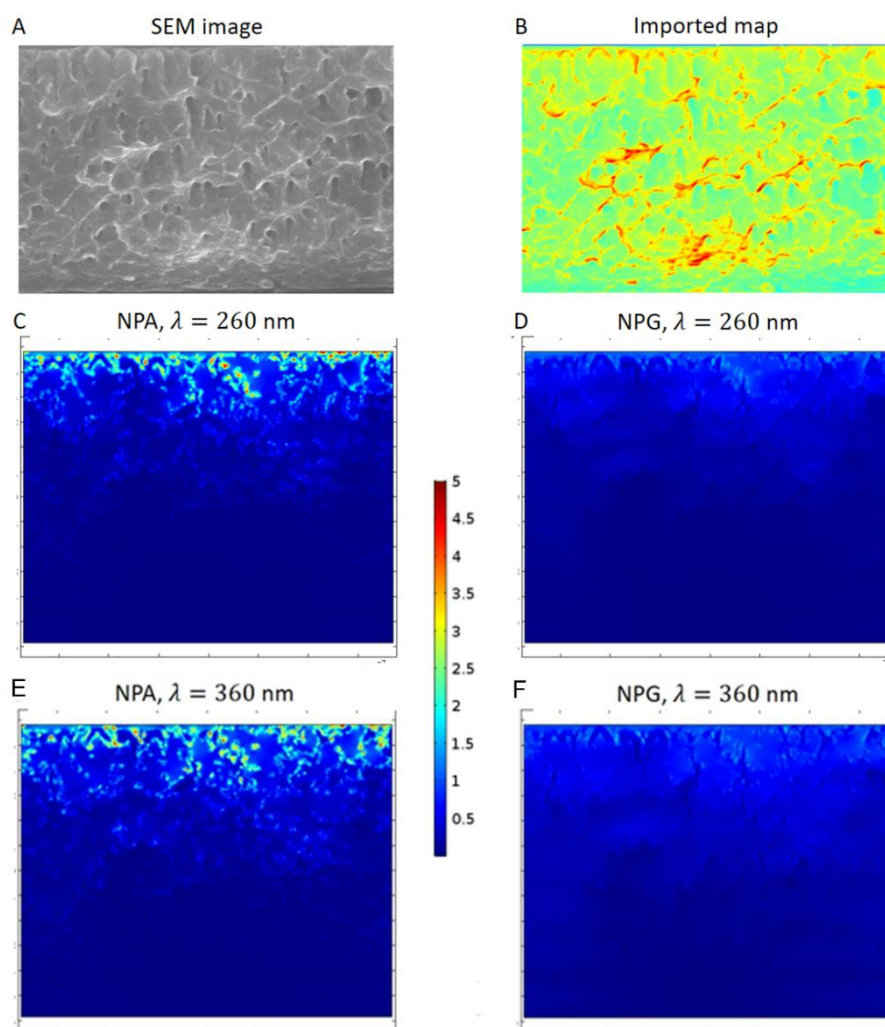


**Figure S16.** *e.m. calculations of field confinement in sample  $A_0$  (same scale) at a wavelength of 260nm (C-D) and 360 nm (E-F) using the optical properties of NPAM and NPG films respectively.*

Figure S17 illustrates the same calculation performed considering the morphology of sample  $C_1$  for wavelength  $\lambda=360$  nm.

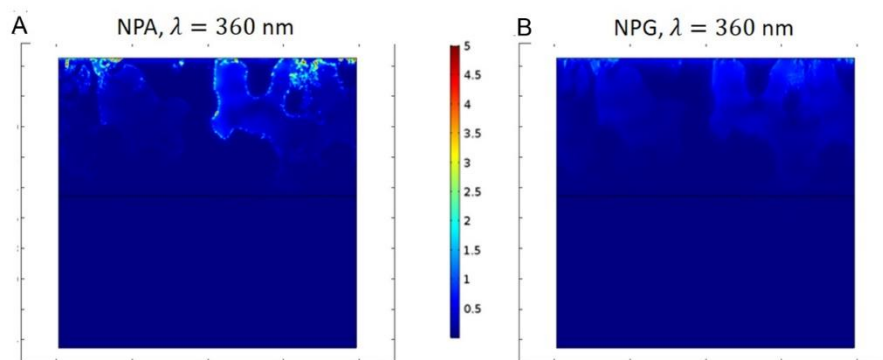


**Figure S17.** *e.m. calculations of field confinement in sample  $C_1$  (same scale) at a wavelength of 360 nm (A-B) using the optical properties of NPAM and NPG films respectively.*

As in Fig. 5, the comparison between the Al-Mg alloy and Au is made so that the imported surface profile is the same for the two cases. The electromagnetic problem is then solved for a similar geometry, where maps of permittivity determine the optical properties of different domains according to what reported in method section in the main text. The same scale is employed to appreciate the much higher efficiency in localising the field around the surface nanoporous and nano-sized asperities of Al-Mg if compared to Au. Indeed, the field enhancement in Fig. S16C-E and S17A reached values of tens, while maxima for NPG, Fig. S16D-F and S17F are roughly 1.8. As for the calculations modelling SERS outcome, these results addressing fluorescence measurements show how the prepared alloy can be more suitable in the UV/DUV range.

In addition, as aforementioned, a threshold parameter  $ths$  has been introduced to assign permittivity values to the domains in the geometry by starting from the imported SEM image of the sample profile. As long as the normalised SEM brightness is greater than  $ths$ , permittivity is the one of the metal – either Au or the alloy – weighted over the image itself (see method section in the main text). As a result, the higher the threshold value, the larger the portion of air at the metal interface. The extreme choice  $ths = 1$  would imply air only in the interface region. Then, Fig. S17A and S17B show field calculations for  $ths = 0.4$ . Instead, here presented the results of the same calculations for a representative alternative value  $ths = 0.6$ .

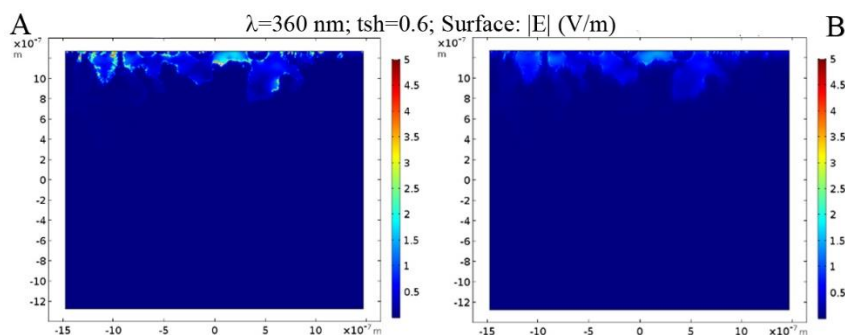


**Figure S18.** *e.m. calculations of field confinement (same scale) at a wavelength of 360 nm using the optical properties of NPAM and NPG films respectively, threshold  $t_{hs}=0.6$ .*

Due to this choice, the field can penetrate more through the structure, as more air is modelled at the surface. The same trend is observed for both NPG and NPAM for a given threshold value.

#### Supporting Note #8 – Time (aging) stability test

Table S3 reports EDS analyses performed on NPAM samples after three months (aging). The stability of oxidation level is confirmed.

**Table S3.** *EDS composition of prepared samples as prepared and after 3 months.*

Sample	Sputtering power for Al-Mg (W) / Treatment	Pristine composition parameter $x$ ( $Al_xMg_{1-x}$ )*	(EDS) Composition After etching (O – Al - Mg)	After 3 months
B <sub>1</sub>	100-85 / 2 min etching	0.23	12% - 23% - 65%	12% - 22 % - 66%
B <sub>2</sub>	100-85 / 5 min etching	0.23	28% - 30% - 42% %	29% - 30% - 41%
C <sub>1</sub>	100-85 / anneal. 5 min etching	0.23	11% - 40% - 49%	12% - 38% - 51%